Boundary Value Problems
a SpringerOpen Journal

RESEARCH Open Access

Time accurate solution to Benjamin–Bona–Mahony–Burgers equation via Taylor–Boubaker series scheme

Mohammad Izadi[1] and Mohammad Esmael Samei[2*]

*Correspondence:
mesamei@gmail.com;
mesamei@basu.ac.ir
[2]Department of Mathematics, Bu-Ali Sina University, Hamedan, Iran
Full list of author information is available at the end of the article

Abstract

The object of this paper is to develop an accurate combined spectral collocation approach to numerically solve the generalized nonlinear Benjamin–Bona–Mahony–Burgers equation. The first stage is devoted to discretization in time, which is carried out with the aid of the well-known Taylor series expansions. Then the spectral collocation procedure based on the Boubaker polynomials is applied for the resulting discretized spatial operator in each time step. A detailed error analysis of the presented technique is carried out with regard to the space variable. The advantages of the hybrid technique are shown via performing several simulations through four test examples. Comparisons between our numerical results and the outcomes of some existing schemes indicate that the proposed technique is not only simple and easy-to-implement, but also sufficiently accurate using a moderate number of bases and a large time step.

MSC: 65M70; 65M12; 65M06

Keywords: Benjamin–Bona–Mahony–Burgers equation; Boubaker polynomials; Collocation points; Second-order accuracy; Taylor expansion

1 Introduction

Diverse important physical phenomena in nature are mathematically described by means of (nonlinear) partial differential equations (PDEs) with appropriate initial and boundary conditions. Except for some particular cases, the closed-form solutions to the most PDEs either do not exist or are not intractable in practice. Thus developing an accurate approximate or numerical solution for nonlinear PDEs becomes practically important in the filed. In the past decades the subject has attracted many authors, and difference equations have been appeared as a promising research field on both applied and theoretical levels (see [1–17]).

The generalized Benjamin–Bona–Mahony–Burgers (BBMB) model (1) was first considered in [1]. Due to the importance and vast applications, many researchers have been considered the BBMB-type equations over the past decades. In this respect, diverse computational and approximation techniques were proposed in the literature. The Galerkin approach was applied to the Benjamin–Bona–Mahony (BBM) equations in [18–20]. The

finite difference schemes with different combined methods in space and time are developed in [6, 7]. The B-spline collocation approaches are studied in [21–23]. The meshless-based methods were investigated in the previously published papers [24, 25]. The spectral collocation procedures based upon (orthogonal) basis functions were discussed in [26–29]. Additionally, a discussion of some other methods for solving PDEs can be found in [30–41]. In most of the proposed numerical solution algorithms for (13), the implemented time marching procedure has the first-order accuracy. In addition, to achieve a reasonable accuracy, the time step cannot be taken rather large. Alternatively, in this research work, we construct a second-order time advancement technique for the numerical treatment of the BBMB equation. Our efficient and accurate approach based upon a hybrid of Taylor method for the time discretization and exponential spectral Boubaker collocation scheme for the spatial operator. The presented hybrid technique is straightforward in implementation compared to other existing numerical models; see also [42–44].

Recently, the authors in [45] obtained new exact solitary solutions for a version of $(3+1)$-dimensional Wazwaz–Benjamin–Bona–Mahony equation formulated in the sense of conformable derivative with the help of two novel techniques: the generalized Kudryashov method and $\exp(-\phi(\aleph))$ method. The general fractional formulation of the Wazwaz–Benjamin–Bona–Mahony equation can be expressed as follows:

$$\mathcal{D}_t^{\zeta}\Psi + \mathcal{D}_x^{\zeta}\Psi + \mathcal{D}_y^{\zeta}\Psi - \mathcal{D}_{xzt}^{\zeta}\Psi = 0,$$

where $\mathcal{D}^{\zeta}$ is the fractional operator of order $0 < \zeta \leq 1$, and the function $\Psi : [0,\infty) \to \mathbb{R}$ is ζ-differentiable at a point t. Matar et al. [46], studied the following fractional differential equation:

$$\begin{cases} \frac{\mathrm{d}}{\mathrm{d}t}(\varphi_p({}^{C}\mathcal{D}^{\alpha,\rho}x(t))) = q(t,x(t),{}^{C}\mathcal{D}^{\gamma,\rho}x(t)), \quad 0 \leq t \leq 1, \\ x(0) + \mu x(1) = \theta_1(x(0),x(1)), \\ x'(1) = \theta_2(x(0),x(1)), \end{cases}$$

where ${}^{C}\mathcal{D}^{\alpha,\rho}$ and ${}^{C}\mathcal{D}^{\gamma,\rho}$ are the generalized Caputo fractional derivatives of orders $0 < \alpha < 1$ and $0 < \gamma < 1$, respectively, $\rho > 1$, and s $q : [0,1] \times \mathbb{R}^2 \to \mathbb{R}$ and $\theta_i : \mathbb{R}^2 \to \mathbb{R}$, $i = 1,2$, are given nonlinear continuous functions. They investigated possible solutions to the following fractional boundary value problem for an implicit nonlinear an implicit nonlinear fractional differential equation:

$$\begin{cases} \mathcal{D}_{0^+}^{q(t)}x(t) = \theta(t,x(t),\mathcal{D}_{0^+}^{q(t)}x(t)), \quad 0 \leq t \leq \Omega, \\ x(0) = 0, \qquad x(\Omega) = 0, \end{cases}$$

where $\Omega > 0$, $q : [0,\Omega] \to (1.2]$ and $\theta : [0,\Omega] \times \mathbb{R}^2 \to \mathbb{R}$ are continuous functions, and $\mathcal{D}_{0^+}^{q(t)}$ is the Riemann–Liouville fractional derivative in the context of variable order $q(t)$ [47]. Matar et al. [48] consider the FDE

$$\begin{cases} \frac{\mathrm{d}}{\mathrm{d}t}(\varphi_p({}^{C}\mathcal{D}^{\varsigma_1,\rho}\wp(t))) = \mathfrak{w}(t,\wp(t),{}^{C}\mathcal{D}^{\varsigma_2,\rho}\wp(t)), \quad t \in [0,1], \\ \wp(0) + \mu\wp(1) = \mathfrak{v}_1(\wp(0),\wp(1)), \quad \mu \neq 1, \\ \wp'(1) = \mathfrak{v}_2(\wp(0),\wp(1)), \end{cases}$$

where ${}^{C}\mathcal{D}^{\varsigma_1,\rho}$ and ${}^{C}\mathcal{D}^{\varsigma_2,\rho}\wp(t)$ are generalized Caputo fractional derivatives of orders $1 < \sigma_1 < 2$ and $0 < \sigma_2 < 1$, respectively, $\rho > 1$, $\varphi_p(p > 1)$ is a p-Laplacian operator, and $\mathfrak{w} : [0,1] \times \mathbb{R}^2 \to \mathbb{R}$ and $\mathfrak{v}_1, \mathfrak{v}_2 : \mathbb{R}^2 \to \mathbb{R}$ are given nonlinear continuous functions. Also, the authors in [49] found a theoretical method to investigate the existence of solutions for the strongly singular fractional model of thermostat control given as

$$\begin{cases} {}^{C}\mathcal{D}^{\omega}x(t) + q(t)\theta(x(t)) = 0, \quad \omega > 0, w \in (n-1, n], \\ x^{(j)} = 0, \quad j = 1, 2, \ldots, n-1, \\ (p(t)x(t))'|_{t=1} + ax(\eta) = 0, \quad a > 0, 0 < \eta < 1, \end{cases}$$

where $(\omega - k - 1)p(1) > a\eta^k$, with $j \neq k$ coupled, $q : [0,1] \to \mathbb{R}$ is singular or strongly singular at some points of $[0,1]$, $p : [0,1] \to [0,\infty)$ is differentiable at $t = 1$, $\theta \in C(\mathbb{R}, \mathbb{R})$, and ${}^{C}\mathcal{D}^{\omega}$ is the Caputo derivative of order ω. For more studied related application, see [50, 51]. Rezapour et al. investigated the multisingular integro-differential pointwise equation

$$\begin{cases} \mathcal{D}_{\mathrm{q}}^{\varsigma}\wp(t) = \mathfrak{w}(t, \wp(t), \wp'(t), \mathcal{D}^{\gamma_1}\wp(t), \mathcal{I}^{\gamma_1}\wp(t)), \quad t \in [0,1], \\ \wp'(0) = \wp(a), \\ \wp(1) = \int_0^b \wp(\xi)\,\mathrm{d}\xi, \end{cases}$$

$\wp^{(j)}(0) = 0, j = 2, \ldots, [\sigma] - 1$, where $\wp \in C^1([0,1])$, $\gamma_1, \gamma_2 \in [2,\infty)$, $a, b \in (0,1)$, $\mathcal{D}^{\varsigma}$ is the Caputo fractional q-derivative of order ς, and $\mathfrak{w} : [0,1] \times \mathbb{R}^4 \to \mathbb{R}$ is a function such that $\mathfrak{w}(t, ., ., ., .)$ is singular at some points $0 \leq t \leq 1$ [52]. In 2021, Izadi [42] presented an effective approximation algorithm to solve the nonlinear Hunter–Saxton equation

$$\begin{cases} w_{xt} + ww_{xx} + 0.5w_x^2 = 0, \\ w|_{t=0} = w_0(x), \end{cases}$$

subjected to the boundary condition $\lim_{x\to\infty} w(x,t) = 0$. Abdelwahed and Chorf [53] consider the nonlinear heat equation: Find a solution φ of

$$\begin{cases} \frac{\partial\varphi}{\partial t} - \operatorname{div}(\lambda(\varphi)\nabla\varphi) = f & \text{in } \Omega\times]0,T[, \\ \varphi(x,t) = 0 & \text{on } \partial\Omega\times]0,T[, \\ \varphi(x,0) = \varphi_0 & \text{in } \partial\Omega, \end{cases}$$

where Ω is a bounded simply connected domain of $\mathbb{R}^d$ $(d = 1,2,3)$, $\partial\Omega$ is its connected Lipschitz continuous boundary, and T is a positive constant. They considered families of large eddy simulation models, which are variants of the classical Smagorinsky model, and similarly to the model of Cottet, Jiroveanu, and Michaux, proposed a selective model based on the local behavior of the angle of the vorticity direction [54].

The chief goal of this research paper is developing an effective time-accurate computational procedure for finding the solutions of a PDE model problem arising in broad branches of science and engineering. We consider a hybrid approximation technique to

numerically treat the following BBMB equation:

$$\begin{aligned}&\frac{\partial w(x,t)}{\partial t}-\mu\frac{\partial^3 w(x,t)}{\partial t\partial x^2}-\gamma\frac{\partial^2 w(x,t)}{\partial x^2}+\sigma\frac{\partial w(x,t)}{\partial x}\\&\quad+\eta w(x,t)\frac{\partial w(x,t)}{\partial x}=h(x,t),\end{aligned}\tag{1}$$

where $x\in[x_L,x_R]$ and $t\in[0,T_f]$. Also, two coefficient parameters μ,γ,σ are positive constants, $\eta\in\mathbb{R}$, and $h(x,t)$ is a familiar real-valued function. Along with this equation, an initial condition is given as

$$w(x,t=0)=w_0(x),\quad x\in[x_L,x_R].\tag{2}$$

Moreover, with the initial-value problem (1)–(2), the following boundary conditions are supplemented:

$$\begin{cases}w(x=x_L,t)=w_L(t),\\w(x=x_R,t)=w_R(t),\end{cases}\tag{3}$$

for $t\in[0,T_f]$, where $w_L(t)$ and $w_R(t)$ are two prescribed functions. If $\gamma=0$, then equation (1) is called the BBM equation, which first studied as a model for the propagation of long waves in nonlinear dispersive systems [2]. Some facts on physical significance of this model were given in [3, 5]. For $\mu=0$ and $\eta=-1$, the model (1) reduces to (generalized) Burgers equation [4].

Our plan in the rest of the paper is as follows. In the next Sect. 2, we illustrate the time advancement procedure for BBMB equation (1), which is relied on the Taylor series expansion. Afterward, in Sect. 3, we give an overview of the Boubaker functions together with some important their properties. In this section, we also discuss the convergence for this class of polynomials. The hybrid strategy of Taylor and Boubaker functions is illustrated in Sect. 4 in detail. The results of numerical simulations presented through tables and figures are given in Sect. 5. We end the paper with the conclusion Sect. 6.

2 Time-marching procedure

To gain an accurate time solution of the nonlinear BBMB equation (1), we first consider the Taylor expansion series to discretize it in time. For this purpose, we uniformly partition the time interval $[0,T_f]$ into J uniform subdivisions. The corresponding grid points and time-step Δt are given by

$$t_0=0<t_1=\Delta t<\cdots<t_J=J\Delta t=T_f,$$

where $\Delta t=t_j-t_{j-1}$, and $j=1,2,\ldots,J$. In what follows, by w^j we denote the approximate solution at time level t_j, that is,

$$w^j(x)\approx w(x,t_j).$$

We then evaluate the original BBMB equation (1) at time level t_j to arrive at

$$\frac{\partial}{\partial t}\left(w^j-\mu\frac{\partial^2 w^j}{\partial x^2}\right)=\gamma\frac{\partial^2 w^j}{\partial x^2}-\sigma\frac{\partial w^j}{\partial x}-\eta w^j\frac{\partial w^j}{\partial x}+h(x,t_j).\tag{4}$$

Let us for convenience define

$$u^j := w^j - \mu \frac{\partial^2 w^j}{\partial x^2}.$$

Application of the Taylor formula to u^j yields

$$\frac{\partial u^j}{\partial t} = \frac{u^{j+1} - u^j}{\Delta t} - \frac{1}{2}\Delta t \frac{\partial^2 u^j}{\partial t^2} + \mathcal{O}\big(\Delta t^2\big). \tag{5}$$

Differentiating (4) with regard to t reveals

$$\frac{\partial^2 u^j}{\partial t^2} = \gamma \frac{\partial^2 w^j}{\partial t \partial x^2} - \sigma \frac{\partial^2 w^j}{\partial t \partial x} - \eta \frac{\partial w^j}{\partial t}\frac{\partial w^j}{\partial x} - \eta w^j \frac{\partial^2 w^j}{\partial t \partial x} + \frac{h(x,t_j)}{\partial t}.$$

Now we replace all first-order derivatives $\frac{\partial w^j}{\partial t}$ by the forward difference relation

$$\frac{w^{j+1} - w^j}{\Delta t}.$$

After multiplying both sides by Δt and some manipulations, the resultant equation becomes

$$\begin{aligned}\Delta t \frac{\partial^2 u^j}{\partial t^2} = {} & \gamma\left(\frac{\partial^2 w^{j+1}}{\partial x^2} - \frac{\partial^2 w^j}{\partial x^2}\right) - \big(\sigma + \eta w^j\big)\left(\frac{\partial w^{j+1}}{\partial x} - \frac{\partial w^j}{\partial x}\right) \\ & - \eta \frac{\partial w^j}{\partial x}\big(w^{j+1} - w^j\big) + h^{j+1} - h^j,\end{aligned} \tag{6}$$

where $h^j := h(x,t_j)$. Our next task is to place (6) into the right-hand side of (5) followed by equating to (4). After multiplying by $2\Delta t$, we get the time-discretized equation for the nonlinear model (1) with second-order accuracy in time. Again for simplicity of notations, we introduce

$$\chi_{j+1}(x) := w^{j+1}(x).$$

Similarly, we define

$$\begin{aligned} a_j(x) &:= -(\gamma \Delta t + 2\mu), \\ b_j(x) &:= \Delta t\big(\eta w^j(x) + \sigma\big), \\ c_j(x) &:= 2 + \Delta t \eta \frac{\partial w^j}{\partial x}(x), \\ f_j(x) &:= 2w^j(x) - [2\mu - \Delta t\gamma]\frac{\partial^2 w^j}{\partial x^2} - \Delta t\sigma \frac{\partial w^j}{\partial x} + \Delta t\big(h^{j+1} + h^j\big). \end{aligned}$$

Therefore the resulting second-order equation with regard to space variable can be written as

$$a_j(x)\chi''_{j+1}(x) + b_j(x)\chi'_{j+1}(x) + c_j(x)\chi_{j+1}(x) = f_j(x), \quad x \in [x_L, x_R], \tag{7}$$

for $j = 0, 1, \ldots, J-1$. In each time level, we must solve the linear equation (7). So we need the given initial condition $w^0 = w_0(x)$ and its first- and second-order derivatives as they appear in the coefficients of (7). In other words, for $j = 0$, we have $\chi_0(x) = w_0(x)$ for $x \in [x_L, x_R]$. At each time level t_{j+1}, we exploit the boundary conditions obtained from (3) at two endpoints $x = x_L, x_R$ as follows:

$$\begin{cases} \chi_{j+1}(x_L) := \chi_L^{j+1} = w_L(t_{j+1}), \\ \chi_{j+1}(x_R) := \chi_R^{j+1} = w_R(t_{j+1}), \end{cases} \tag{8}$$

for $j = 0, 1, \ldots, J-1$.

3 Boubaker functions: an overview

The family of nonorthogonal Boubaker polynomials $\mathcal{B}_\ell(x)$ naturally appeared in the study of heat transfer equation when its solution can be expanded in terms of Bessel functions of the first kind [55]. These polynomials are very closely related to the Chebyshev polynomials $\mathrm{U}_\ell(x)$ of the second kind denoted by the relation

$$\mathcal{B}_\ell(x) = \mathrm{U}_\ell\left(\frac{x}{2}\right) + 3\mathrm{U}_{\ell-2}\left(\frac{x}{2}\right).$$

These polynomials are obtained via the following recursive formula:

$$\mathcal{B}_\ell(x) = x\mathcal{B}_{\ell-1}(x) - \mathcal{B}_{\ell-2}(x), \quad \ell = 3, 4, \ldots, \tag{9}$$

where the first three Boubaker functions are $\mathcal{B}_0(x) = 1$, $\mathcal{B}_1(x) = x$, and

$$\mathcal{B}_2(x) = x^2 + 2.$$

For $\ell > 0$, these functions are the unique solutions of the second-order differential equation

$$\begin{aligned} &\big(x^2-1\big)\big(3\ell x^2 + \ell - 2\big)y'' + 3x\big(\ell x^2 + 3\ell - 2\big)y' \\ &\quad - \ell\big(3\ell^2 x^2 + \ell^2 - 6\ell + 8\big)y = 0 \quad (\ell \in \mathbb{N}), \end{aligned} \tag{10}$$

where $y(x) = \mathcal{B}_\ell(x)$. Furthermore, the explicit series solution of Boubaker polynomial $\mathcal{B}_\ell(x)$ of degree ℓ is given by

$$\mathcal{B}_\ell(x) = \sum_{r=0}^{\lfloor \frac{\ell}{2} \rfloor} (-1)^r \binom{\ell - r}{r} \frac{\ell - 4r}{\ell - r} x^{\ell-2r} \quad (\ell > 1). \tag{11}$$

The next theorem establishes the distribution of the zeros of these polynomials on $[-2, 2]$; see [56, Theorem 2.4].

Theorem 3.1 *The function $\mathcal{B}_\ell(x)$ of degree ℓ has has $\ell - 2$ real zeros and two nonreal, purely imaginary complex zeros. All zeros of $\mathcal{B}_\ell(x)$ are located in $[-2, 2]$, and the two purely imaginary zeros lie outside the unit circle.*

Remark 3.1 Based on the observation established in Theorem 3.1, the shifted version of these polynomials were previously considered on an arbitrary domain $[x_L, x_R]$ in [57]. This can be accomplished trough the change of variable

$$\eta = \frac{4x - 2(x_L + x_R)}{x_R - x_L},$$

where $x \in [x_L, x_R]$ and $\eta \in [-2, 2]$. Thus we get the shifted version of these polynomial by using $\mathcal{B}^*_\ell(\eta) = \mathcal{B}_\ell(x)$. In the numerical examples, we may appropriately use the shifted Boubaker polynomials.

3.1 Convergence results

To proceed, we define $\Omega = [x_L, x_R]$ and the related weighted L_2 space as [57]

$$L_{2,\omega}(\Omega) = \big\{s : \Omega \to \mathbb{R} | s \text{ is measurable, and } \|s\|_\omega < \infty\big\},$$

where

$$\|s\|^2_\omega = \int_{x_L}^{x_R} \big|s(x)\big|^2 \omega(x)\,\mathrm{d}x$$

with $\omega(x) = \frac{1}{x_R - x_L}$ denotes the induced norm resulting from the following inner product of the space $L_{2,\omega}(\Omega)$:

$$\big\langle s(x), p(x)\big\rangle_\omega = \int_{x_L}^{x_R} s(x)p(x)\omega(x)\,\mathrm{d}x.$$

In practice, we consider a finite-dimensional subspace of $L_{2,\omega}(\Omega)$ of the form

$$\mathbb{L}_M = \mathrm{span}\big\langle \mathcal{B}^*_0(x), \mathcal{B}^*_1(x), \ldots, \mathcal{B}^*_M(x)\big\rangle.$$

Clearly, $\dim(\mathbb{L}_M) = M + 1$, and $\mathbb{L}_M$ is a closed and thus complete subspace of $L_{2,\omega}(\Omega)$. Thus any function $u \in L_{2,\omega}(\Omega)$ has a unique best approximation $u^* \in \mathbb{L}_M$ in the sense that

$$\big\|u(x) - u^*(x)\big\|_\omega \le \big\|u(x) - v(x)\big\|_\omega \quad \forall v \in \mathbb{L}_M. \tag{12}$$

We further invoke the following result from the approximation theory [58].

Theorem 3.2 *Let u be an M times continuously differentiable function on Ω. Also, let P_M denote the interpolating function of u at M Chebyshev nodes in the interval Ω. Then, for every $x \in \Omega$, we have*

$$\big|u(x) - P_M(x)\big| \le \frac{(x_R - x_L)^M \|u\|_\infty}{2^{2M-1} M!},$$

where $\|u\|_\infty := \max_{x\in\Omega} |u^{(M)}(x)|$.

Now assume that an arbitrary function $u \in L_{2,\omega}(\Omega)$ can be written in terms of shifted Boubaker functions as

$$u(x) = \sum_{\ell=0}^{\infty} \lambda_\ell \mathcal{B}_\ell^*(x).$$

By restricting our attention to the finite subsets $\mathbb{L}_M$ of $L_{2,\omega}(\Omega)$ we may write a truncated series for u as

$$u(x) \approx u_M(x) = \sum_{\ell=0}^{M} \lambda_\ell \mathcal{B}_\ell^*(x).$$

The next theorem provides an error bound for $E_M(x) = u(x) - u_M(x)$.

Theorem 3.3 *Let*

$$u \in C^{(M+1)}(\Omega) \cap L_{2,\omega}(\Omega).$$

Let u_M be the best approximation to u in the space $\mathbb{L}_M$ in the sense of (12). *Then we have*

$$\left\| E_M(x) \right\|_\omega \to 0$$

as $M \to \infty$.

Proof Since u_M is the best approximation belonging to $\mathbb{L}_M$, we obtain

$$\left\| E_M(x) \right\|_\omega^2 = \left\| u(x) - u_M(x) \right\|_\omega^2 \leq \left\| u(x) - v(x) \right\|_\omega^2 \quad \forall v \in \mathbb{L}_M.$$

The foregoing inequality is valid in particular for $v = P \in \mathbb{L}_M$. We therefore conclude that

$$\left\| E_M(x) \right\|_\omega^2 \leq \left\| u(x) - P_{M+1}(x) \right\|_\omega^2 = \int_\Omega \left| u(x) - P_{M+1}(x) \right|^2 \omega(x)\, \mathrm{d}x.$$

According to Theorem 3.2 with $(M+1)$ nodes, we get

$$\begin{aligned} \left\| E_M(x) \right\|_\omega^2 &\leq \int_{x_L}^{x_R} \left| \frac{\|u\|_\infty (x_R - x_L)^{M+1}}{(M+1)! 2^{2M+1}} \right|^2 \omega(x)\, \mathrm{d}x \\ &\leq \left[\frac{\|u\|_\infty (x_R - x_L)^{M+1}}{(M+1)! 2^{2M+1}} \right]^2. \end{aligned}$$

The proof is finished by tending M to infinity. □

4 The hybrid procedure

The discretization of the BBMB equation (1) with regard to time is already carried out by relation (7). Also, the given boundary conditions (3) are converted to the boundary conditions (8) for the second-order differential equation (7). So the main objective is to treat the initial-boundary value problem (7)–(8) numerically with respect to the space variable x. Suppose that the solutions $\chi_{j+1}(x)$ of (7) at each time level j can be written as

combinations of the (shifted) Boubaker functions defined by (11). Let assume that $\mathcal{X}_{j,M}(x)$ are the computed Boubaker approximations to $\chi_j(x)$ at the time steps t_j. To start, we need $\chi_0(x)$, which can be derived from the given initial condition $w_0(x)$. In the next time step t_{j+1}, we look for the approximate solution $\mathcal{X}_{j+1,M}(x)$ for $j = 0, 1, \ldots, J-1$ as follows:

$$\mathcal{X}_{j+1,M}(x) = \sum_{\ell=0}^{M} \lambda_\ell^{j+1} \mathcal{B}_\ell(x), \quad x \in \Omega. \tag{13}$$

Here our ultimate goal is to find the unknowns λ_ℓ^{j+1} for $\ell = 0, 1, \ldots, M$ at time level $j \geq 0$. For convenience, we set

$$\boldsymbol{O}_M(x) = \begin{bmatrix} \mathcal{B}_0(x) & \mathcal{B}_1(x) & \ldots & \mathcal{B}_M(x) \end{bmatrix},$$
$$\boldsymbol{\Lambda}_M^{j+1} = \begin{bmatrix} \lambda_0^{k+1} & \lambda_1^{k+1} & \ldots & \lambda_M^{k+1} \end{bmatrix}^T.$$

With the aid of these vectors, the $(M+1)$-term finite expansion series (13) can be expressed compactly in the matrix form as

$$\mathcal{X}_{j+1,M}(x) = \boldsymbol{O}_M(x) \boldsymbol{\Lambda}_M^{j+1}. \tag{14}$$

After defining the vector of monomials

$$\boldsymbol{V}_M(x) = \begin{bmatrix} 1 & x & x^2 & \ldots & x^M \end{bmatrix},$$

we further decompose the vector of Boubaker bases as

$$\boldsymbol{O}_M(x) = \boldsymbol{V}_M(x) \boldsymbol{N}_M, \tag{15}$$

where the upper-triangular matrix

$$\boldsymbol{N}_M = (n_{i,j})_{i=j-2\lfloor \frac{j}{2} \rfloor, j=2}^{M} \quad (i \leq j)$$

has the following elements:

$$n_{j,i} := \begin{cases} (-1)^{\frac{i-j}{2}} \left(\frac{4j-2i}{i+j}\right) \frac{\Gamma(\frac{i+j}{2}+1)}{\Gamma(j+1)\Gamma(\frac{i-j}{2}+1)} & \text{if } (i-j) \text{ is even,} \\ 0 & \text{if } (i-j) \text{ is odd or } i > j, \\ 1 & \text{if } i = j, \end{cases}$$

where the only nonzero elements on the first and second columns are $n_{0,0}, n_{1,1} = 1$. For example, for $M = 6$, we get

$$\boldsymbol{N}_6 = \begin{pmatrix} 1 & 0 & 2 & 0 & -2 & 0 & 2 \\ 0 & 1 & 0 & 1 & 0 & -3 & 0 \\ 0 & 0 & 1 & 0 & 0 & 0 & -3 \\ 0 & 0 & 0 & 1 & 0 & -1 & 0 \\ 0 & 0 & 0 & 0 & 1 & 0 & -2 \\ 0 & 0 & 0 & 0 & 0 & 1 & 0 \\ 0 & 0 & 0 & 0 & 0 & 0 & 1 \end{pmatrix}.$$

We note that determinant of $\boldsymbol{N}_M$ is equal to unity. Ultimately, we requires a set of collocation points on $[x_L, x_R]$ to acquire an approximate solution of the discretized model problem (7) in the form (9). In this respect, we use the zeros of the shifted Chebyshev polynomials on $[x_L, x_R]$ given by

$$x_\tau = \frac{x_L + x_R}{2} + \frac{x_R - x_L}{2} s_\tau, \quad \tau = 0, 1, \ldots, M, \tag{16}$$

where s_τ are roots of Chebyshev functions of degree $(M+1)$ on $(-1, 1)$. Further, we combine relationships (14) and (15) to express the approximate solution $\mathcal{X}_{j+1,M}(x)$ in (13) in a compact form as

$$\mathcal{X}_{j+1,M}(x) = \boldsymbol{O}_M(x)\boldsymbol{\Lambda}_M^{j+1} = \boldsymbol{V}_M(x)\boldsymbol{N}_M\boldsymbol{\Lambda}_M^{j+1}. \tag{17}$$

Using points of collocation (16) and putting them into (17), we obtain

$$\boldsymbol{X}_{j+1} = \boldsymbol{V}\boldsymbol{N}_M\boldsymbol{\Lambda}_M^{j+1}, \qquad \boldsymbol{X}_{j+1} = \begin{pmatrix} \mathcal{X}_{j+1,M}(x_0) \\ \mathcal{X}_{j+1,M}(x_1) \\ \vdots \\ \mathcal{X}_{j+1,M}(x_M) \end{pmatrix}, \qquad \boldsymbol{V} = \begin{pmatrix} \boldsymbol{V}_M(x_0) \\ \boldsymbol{V}_M(x_1) \\ \vdots \\ \boldsymbol{V}_M(x_M) \end{pmatrix}. \tag{18}$$

The next objective would be finding a connection between $\boldsymbol{V}_M(x)$ and its derivatives. We can show that the derivatives of $\boldsymbol{V}_M(x)$ can be stated in terms of differentiation matrix $\boldsymbol{D}$ as

$$\frac{d^k}{dx^k}\boldsymbol{V}_M(x) = \boldsymbol{V}_M(x)\boldsymbol{E}, \qquad \boldsymbol{E} = \begin{pmatrix} 0 & 1 & 0 & \ldots & 0 \\ 0 & 0 & 2 & \ldots & 0 \\ \vdots & \vdots & \ddots & \vdots & \vdots \\ 0 & 0 & 0 & \ddots & M \\ 0 & 0 & 0 & \ldots & 0 \end{pmatrix}_{(M+1)\times(M+1)}, \tag{19}$$

for $k = 1, 2$. Twice differentiation of relation (17) with respect to x and using the former relation (19) reveal that

$$\begin{cases} \chi'_{j+1}(x) \approx \mathcal{X}^{(1)}_{j+1,M}(x) = \boldsymbol{V}_M(x)\boldsymbol{E}\boldsymbol{N}_M\boldsymbol{\Lambda}_M^{j+1}, \\ \chi''_{j+1}(x) \approx \mathcal{X}^{(2)}_{j+1,M}(x) = \boldsymbol{V}_M(x)\boldsymbol{E}^2\boldsymbol{N}_M\boldsymbol{\Lambda}_M^{j+1}. \end{cases} \tag{20}$$

Now it is sufficient to insert the points of collocations (16) into the last formulas to obtain the following matrix expressions for the first and second derivatives in (7):

$$\boldsymbol{X}^{(1)}_{j+1} = \boldsymbol{V}\boldsymbol{E}\boldsymbol{N}_M\boldsymbol{\Lambda}_M^{j+1}, \qquad \boldsymbol{X}^{(1)}_{j+1} = \begin{pmatrix} \mathcal{X}^{(1)}_{j+1,M}(x_0) \\ \mathcal{X}^{(1)}_{j+1,M}(x_1) \\ \vdots \\ \mathcal{X}^{(1)}_{j+1,M}(x_M) \end{pmatrix}, \tag{21}$$

$$\boldsymbol{X}_{j+1}^{(2)} = \boldsymbol{V}\boldsymbol{E}^2\boldsymbol{N}_M\boldsymbol{\Lambda}_M^{j+1}, \qquad \boldsymbol{X}_{j+1}^{(2)} = \begin{pmatrix} \mathcal{X}_{j+1,M}^{(2)}(x_0) \\ \mathcal{X}_{j+1,M}^{(2)}(x_1) \\ \vdots \\ \mathcal{X}_{j+1,M}^{(2)}(x_M) \end{pmatrix}. \tag{22}$$

If we substitute the approximate solution $\mathcal{X}_{j+1,M}(x)$ and its two derivatives

$$\mathcal{X}_{j+1,M}^{(1)}(x), \qquad \mathcal{X}_{j+1,M}^{(2)}(x)$$

into (7), then the resulting equation for $j = 0, 1, \ldots, J-1$ is

$$a_j(x)\mathcal{X}_{j+1,M}^{(2)}(x) + b_j(x)\mathcal{X}_{j+1,M}^{(1)}(x) + c_j(x)\mathcal{X}_{j+1,M}(x) = f_j(x) \tag{23}$$

for $x \in [x_L, x_R]$. Inserting the collocation points inserted into the foregoing equation followed by writing it in a matrix representation yields

$$\boldsymbol{A}\boldsymbol{X}_{j+1}^{(2)} + \boldsymbol{B}\boldsymbol{X}_{j+1}^{(1)} + \boldsymbol{C}\boldsymbol{X}_{j+1} = \boldsymbol{F}_j, \quad j = 0, 1, \ldots, J-1, \tag{24}$$

where we have used the coefficient matrices $\boldsymbol{A}_j$ ($\boldsymbol{B}_j$ or $\boldsymbol{C}_j$) of size $(M+1) \times (M+1)$ and the vectors $\boldsymbol{F}_j$ of size $(M+1) \times 1$ defined as

$$\boldsymbol{A}_j(\boldsymbol{B}_j \text{ or } \boldsymbol{C}_j) = \begin{pmatrix} a_j(b_j \text{ or } c_j)(x_0) & 0 & \ldots & 0 \\ 0 & a_j(b_j \text{ or } c_j) & \ldots & 0 \\ \vdots & \vdots & \ddots & \vdots \\ 0 & 0 & \ldots & a_j(b_j \text{ or } c_j)(x_M) \end{pmatrix},$$

$$\boldsymbol{F}_j = \begin{pmatrix} f_j(x_0) \\ f_j(x_1) \\ \vdots \\ f_j(x_M) \end{pmatrix}.$$

Based on the matrix forms derived in relations (18)–(22), we get the fundamental matrix equation

$$\boldsymbol{Y}_j\boldsymbol{\Lambda}_M^{j+1} = \boldsymbol{F}_j, \qquad [\boldsymbol{Y}_j; \boldsymbol{F}_j], \tag{25}$$

where

$$\boldsymbol{Y}_j := \left\{\boldsymbol{A}_j\boldsymbol{V}\boldsymbol{E}^2 + \boldsymbol{B}_j\boldsymbol{V}\boldsymbol{E} + \boldsymbol{C}_j\boldsymbol{V}\right\}\boldsymbol{N}_M.$$

To obtain the unknowns $\lambda_0^{j+1}, \lambda_1^{j+1}, \ldots, \lambda_M^{j+1}$, we may use any linear solver to solve the matrix equation (25) consisting of $M+1$ linear equations and $M+1$ unknowns. The incorporation of the boundary conditions (8) into the fundamental matrix equation (25) is still demanding to get a unique solution. By means of representation (15) the boundary conditions $\mathcal{X}_{j+1,M}(x_L) = \chi_L^{j+1}$ and $\mathcal{X}_{j+1,M}(x_R) = \chi_R^{j+1}$ can be written in the matrix notation:

$$\overline{\boldsymbol{Y}}_{L,j}\boldsymbol{\Lambda}_M^{j+1} = \chi_L^{j+1}, \qquad \overline{\boldsymbol{Y}}_{L,j} := \boldsymbol{V}_M(x_L)\boldsymbol{N}_M = [\bar{y}_{L,0} \quad \bar{y}_{L,1} \quad \ldots \quad \bar{y}_{L,M}],$$

$$\overline{\boldsymbol{Y}}_{R,j}\boldsymbol{\Lambda}_M^{j+1} = \chi_R^{j+1}, \qquad \overline{\boldsymbol{Y}}_{R,j} := \boldsymbol{V}_M(x_R)\boldsymbol{N}_M = [\bar{y}_{R,0} \quad \bar{y}_{R,0} \quad \dots \quad \bar{y}_{R,0}].$$

After the replacements of two rows (first and last rows) of the augmented matrix $[\boldsymbol{Y}_j;\boldsymbol{F}_j]$ by two row matrices $[\overline{\boldsymbol{Y}}_{L,j};\chi_L^{j+1}]$ and $[\overline{\boldsymbol{Y}}_{L,j};\chi_R^{j+1}]$, we get the linear algebraic system of equations

$$[\overline{\boldsymbol{Y}}_j;\overline{\boldsymbol{F}}_j] = \begin{pmatrix} \bar{y}_{L,0} & \bar{y}_{L,1} & \bar{y}_{L,2} & \bar{y}_{L,3} & \cdots & \bar{y}_{L,M} & ; & \chi_L^{j+1} \\ \bar{y}_{1,0} & \bar{y}_{1,1} & \bar{y}_{1,2} & \bar{y}_{1,3} & \cdots & \bar{y}_{1,M} & ; & F_j(x_1) \\ \bar{y}_{2,0} & \bar{y}_{2,1} & \bar{y}_{2,2} & \bar{y}_{2,3} & \cdots & \bar{y}_{2,M} & ; & F_j(x_2) \\ \vdots & \vdots & \vdots & \ddots & \vdots & \vdots & ; & \vdots \\ \bar{y}_{M-1,0} & \bar{y}_{M-1,1} & \bar{y}_{M-1,2} & \bar{y}_{M-1,3} & \cdots & \bar{y}_{M-1,M} & ; & F_j(x_{M-1}) \\ \bar{y}_{R,0} & \bar{y}_1 & \bar{y}_{R,1} & \bar{y}_{R,3} & \cdots & \bar{y}_{R,M} & ; & \chi_R^{j+1} \end{pmatrix}. \tag{26}$$

Ultimately, once the above linear system is solved, we get the unknown Boubaker coefficients in (13) or (17).

5 Graphical and experimental results

We performed some numerical experiments to testify the exactness of theoretical findings as well as the practicability and utility of the presented hybrid algorithm for the model problem (1) with initial and boundary conditions (2)–(3). Our calculations were performed utilizing Matlab 2021a on a laptop computer with a 2.2 GHz Intel Core i7 CPU and 16 GB memory.

Additionally, the numerical errors are assessed by defining the (pointwise) absolute errors at time step $t = t_j$ via

$$E_{j,M}(x) := \left|w(x,t_j) - \mathcal{X}_{j,M}(x)\right|, \quad x \in [x_L,x_R] \ (j = 1,\dots,J).$$

The calculation of the L_2 and the L_∞ error norms at $t = T_f$ are accomplished through defining

$$\mathcal{E}_\infty := \max_{x_L \le x \le x_R} E_{J,M}(x),$$
$$\mathcal{E}_2 := \left(\int_{x_L}^{x_R} \frac{[w(x,T_f) - \mathcal{X}_{J,M}(x)]^2}{M+1}\,\mathrm{d}x\right)^{1/2}.$$

Furthermore, the estimated rates of convergence of $\mathcal{E}_\infty$ and $\mathcal{E}_2$ are calculated as the the number bases and grid size are halved successively. Suppose that $\mathcal{E}_\ell \equiv \mathcal{E}_\ell(J,M)$ for $\ell = 2,\infty$. Then the rates of convergence (ROCs) with regard to x and t are estimated as

$$\mathrm{ROCx}_\ell := \log_2 \frac{\mathcal{E}_\ell(J,2M)}{\mathcal{E}_\ell(J,M)},$$
$$\mathrm{ROCt}_\ell := \log_2 \frac{\mathcal{E}_\ell(J,M)}{\mathcal{E}_\ell(2J,M)}, \quad \ell = 2,\infty.$$

Test Problem 5.1 *We first consider* (1) *using the following coefficients and right-hand side* [7]: $\mu = 1, \gamma = 1, \sigma = 1, \eta = 1,$

$$h(x,t) = \pi e^{-2t}\sin(2\pi x) + 2\pi e^{-t}\cos(2\pi x) - e^{-t}\sin(2\pi x).$$

The given periodic initial and boundary conditions are

$$\begin{cases} w(x,0) = \sin(2\pi x), \\ w(x_L,t) = 0, \\ w(x_L,t) = 0, \quad [x_L,x_R] = [0,1]. \end{cases}$$

The exact analytical solution takes the form

$$w(x,t) = e^{-t}\sin(2\pi x), \quad x \in [0,1], t \in [0,T_f].$$

We first consider $\Delta t = 0.1$ and $T_f = 1$. We use (13) with $M = 8$ to obtain the following approximate solutions at the first and last time steps $t = \Delta t$ and $t = T_f$ for $0 \le x \le 1$:

$$\begin{aligned} \mathcal{X}_{1,8}(x) = {} & -0.0253645x^8 + 51.0847x^7 - 178.607x^6 \\ & + 197.218x^5 - 46.6584x^4 - 27.7309x^3 \\ & - 1.00867x^2 + 5.72667x - 3.48812 \times 10^{-105} \end{aligned}$$

and

$$\begin{aligned} \mathcal{X}_{10,8}(x) = {} & -0.210542x^8 + 21.5219x^7 - 73.7469x^6 \\ & + 81.07x^5 - 19.3787x^4 - 11.1573x^3 \\ & - 0.426105x^2 + 2.3278x. \end{aligned}$$

The profile of the approximate solution using these parameters are presented in Fig. 1, left. In Fig. 1, right, we further present the achieved absolute errors $E_{j,M}(x)$ for $x \in [0,1]$, $\Delta t = 0.1$, and $T_f = 1$, evaluated at various time levels

$$t_j = j\Delta t, \quad j = 1,2,\ldots,10.$$

In Tables 1 and 2, some comparisons are done to validate our computational results.

For this purpose, the error norms in the L_∞ evaluated at the final time $t = T_f$ are calculated. In Table 1 the spatial rate of convergence of the proposed hybrid technique for a moderate time step $\Delta t = 0.01$ and some

$$M = 2^i, \quad i = 1,2,3,4,$$

are reported. In addition, the elapsed CPU time (in seconds) are further presented in Table 1. It should be emphasized that in each case the required times for solving the modified linear system of equations (26) in all time steps are added together. Here we have 100 time steps. Moreover, analogue results obtained by the fourth-order difference method (FODM) [7] using the parameters $k = 10^{-4}$ and different

$$h = \frac{0.1}{2^i}, \quad i = 0,1,2,3,$$

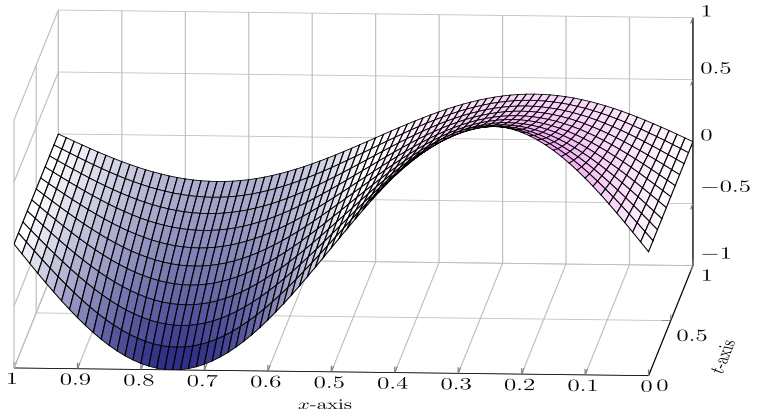

(a) Approximate solution

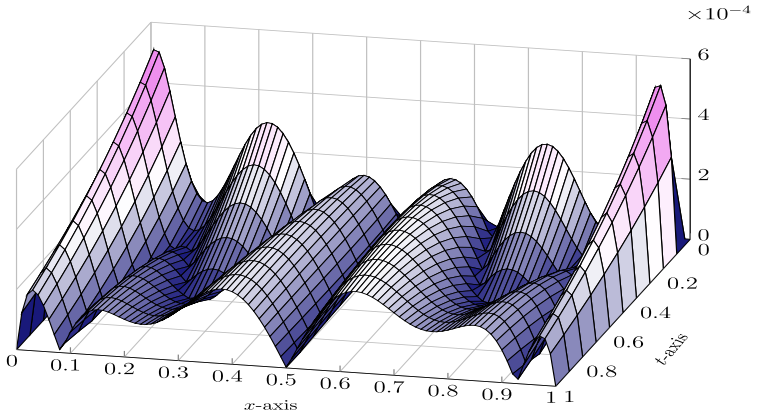

(b) Absolute errors

Figure 1 Graphs of approximate solution (**a**) and absolute errors (**b**) in Test Problem 5.1 for $\Delta t = 0.1, M = 8$, and $T_f = 1$

are tabulated in Table 1. We can clearly see that the performance of the proposed hybrid technique is better than the FODM with less computational efforts and the number of bases.

The second-order accuracy of the present technique with respect to time variable is investigated in Table 2. In this respect, we use a fixed $M = 10$ and various

$$\Delta t = \frac{1}{2^i}, \quad i = 1, 2, 3, 4.$$

The related outcomes of the existing FODM [7] are also presented in Table 2 for comparison. Obviously, our method with considerably larger time steps Δt shows its order of accuracy as $\mathcal{O}(\Delta t^2)$ in comparison with FODM.

Finally, for this example, we go beyond the unit time interval and consider $T_f = 3\pi$. In this case the approximate solutions at time $t = T_f$ is given by

$$\begin{aligned}\mathcal{X}_{94,10}(x) = {} & 0.000214278x^{10} - 0.00364302x^9 + 0.0137945x^8 \\ & - 0.0196859x^7 + 0.00787041x^6 + 0.00367164x^5\end{aligned}$$

Table 1 The results of L_∞ error norms, CPU times, and the related spatial rate of convergence in Test Problem 5.1 with $\Delta t = 0.01$ and diverse M

M	Taylor–Boubaker ($\Delta t = 10^{-2}$)			FODM [7] ($k = 10^{-4}$)		
	$\mathcal{E}_\infty$	ROCx_∞	CPU(s)	h	$e_\infty(h,k)$	Order_h
2	5.788417×10^{-1}	–	16.8013	$\frac{1}{10}$	4.612813×10^{-4}	–
4	9.243067×10^{-2}	2.6467	20.1999	$\frac{1}{20}$	3.103213×10^{-5}	3.893812
8	2.426774×10^{-4}	8.5732	27.4852	$\frac{1}{40}$	1.980428×10^{-6}	3.969878
16	3.371226×10^{-6}	6.1696	45.2692	$\frac{1}{80}$	1.244767×10^{-7}	3.991864

Table 2 The results of L_∞ error norms, CPU times, and the related temporal rate of convergence in Test Problem 5.1 with $M = 10$ and diverse Δt

Δt	Taylor–Boubaker ($M = 10$)			FODM [7] ($h = 10^{-3}$)		
	$\mathcal{E}_\infty$	ROCt_∞	CPU(s)	k	$e_\infty(h,k)$	Order_k
$\frac{1}{2}$	8.620986×10^{-3}	–	0.47193	$\frac{1}{10}$	3.117640×10^{-4}	–
$\frac{1}{4}$	2.119906×10^{-3}	2.0239	0.94799	$\frac{1}{20}$	7.787890×10^{-5}	2.001150
$\frac{1}{8}$	5.286064×10^{-4}	2.0037	1.89863	$\frac{1}{40}$	1.946593×10^{-5}	2.000280
$\frac{1}{16}$	1.328693×10^{-4}	1.9922	3.80004	$\frac{1}{80}$	4.866066×10^{-6}	2.000123

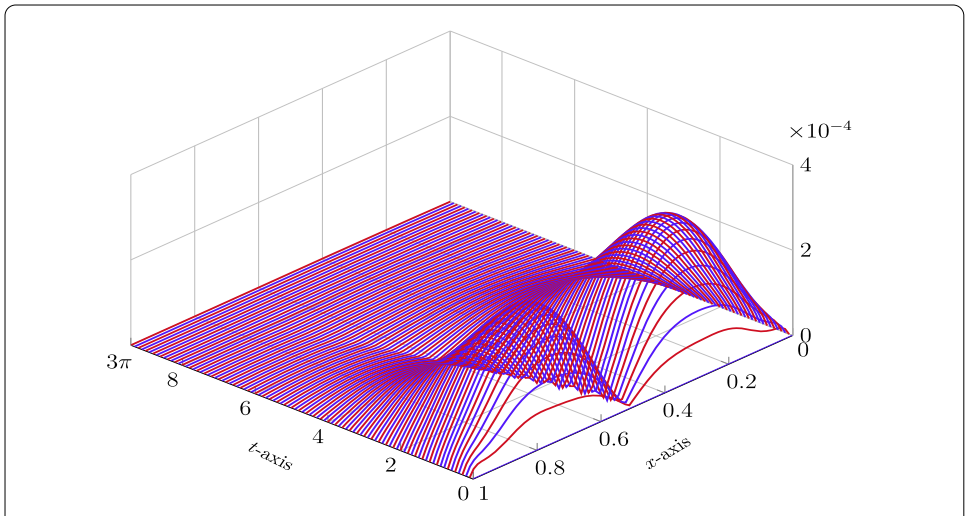

Figure 2 Plot of numerical solutions in Test Problem 5.1 at diverse time instants $t = \ell \Delta t, \ell = 1, 2, \ldots, \lfloor 30\pi \rfloor$, for $\Delta t = 0.1, M = 10$, and $T_f = 3\pi$

$$+ 0.000685197x^4 - 0.00340879x^3 - 0.00000189864x^2$$
$$+ 0.000503632x - 5.32245 \times 10^{-110}.$$

Here we have used $\Delta t = 0.1$ and $M = 10$. The achieved absolute errors $E_{j,10}(x)$ at all time steps are depicted in Fig. 2.

Test Problem 5.2 *As the second test problem, let us consider* [6, 27, 28] $\mu = 1, \gamma = 1, \sigma = 1, \eta = 1$,

$$h(x,t) = e^{-t}\cos(x) - e^{-t}\sin(x) + \frac{e^{-2t}}{2}\sin(2x).$$

The initial and boundary conditions are taken for $x \in [x_L, x_R] = [0, \pi]$ *and* $t \in [0, T_f]$ *as*

$$\begin{cases} w(x,0) = \sin(x), \\ w(x_L,t) = 0, \\ w(x_R,t) = 0. \end{cases}$$

The exact solution for this model problem is

$$w(x,t) = e^{-t}\sin(x).$$

Let us first consider $\Delta t = 0.1$, $T_f = 1, 2, 4$, *and* $T_f = 10$. *The approximated solutions using* $M = 8$ *obtained at these* $t = T_f$ *are given as follows*:

$$\begin{aligned} \mathcal{X}_{10,8}(x) &= 9.3804 \times 10^{-6}x^8 - 1.1566 \times 10^{-4}x^7 + 1.0527 \times 10^{-4}x^6 \\ &\quad + 0.00293115x^5 + 1.3398 \times 10^{-4}x^4 - 0.0614951x^3 \\ &\quad - 2.3178 \times 10^{-5}x^2 + 0.367838x + 1.70 \times 10^{-8}, \\ \mathcal{X}_{20,8}(x) &= 3.8074 \times 10^{-6}x^8 - 4.7055 \times 10^{-5}x^7 + 5.8875 \times 10^{-5}x^6 \\ &\quad + 1.0406 \times 10^{-3}x^5 + 8.5359 \times 10^{-5}x^4 - 0.02265x^3 \\ &\quad - 1.0890 \times 10^{-6}x^2 + 0.135264x, \\ \mathcal{X}_{40,8}(x) &= 5.6989 \times 10^{-7}x^8 - 7.2805 \times 10^{-6}x^7 + 1.3162 \times 10^{-5}x^6 \\ &\quad + 1.2898 \times 10^{-4}x^5 + 2.4261 \times 10^{-5}x^4 - 0.00307087x^3 \\ &\quad - 1.4795 \times 10^{-5}x^2 + 0.0182886x \end{aligned}$$

and

$$\begin{aligned} \mathcal{X}_{100,8}(x) &= 3.3011 \times 10^{-10}x^8 - 7.4345 \times 10^{-9}x^7 + 1.2907 \times 10^{-8}x^6 \\ &\quad + 3.3227 \times 10^{-7}x^5 + 5.6666 \times 10^{-8}x^4 - 7.7921 \times 10^{-6}x^3 \\ &\quad - 1.5728 \times 10^{-7}x^2 + 4.5477 \times 10^{-6}x. \end{aligned}$$

Graphics of the whole approximate solutions on $(x,t) \in [0,\pi] \times [0, T_f]$ *using various* $T_f = 1, 2, 4, 10$ *are presented in Figs*. 3 *and* 4. *The maximum absolute errors in all four cases is are than* $\mathcal{E}_\infty = 5 \times 10^{-5}$. *However, to get more accurate results, we may use a smaller time step* Δt *or increase the number of bases* M. *To show this fact, we utilize* $M = 8$ *and set* $\Delta t = 0.01$. *The snapshots of absolute errors at all time steps*

$$t = s\Delta t, \quad s = 1, \ldots, 1000,$$

are visualized in Fig. 5.

A comparison of the outcomes obtained by the present Taylor–Boubaker method (*TBM*) *with the outcomes of some existing approaches are carried out in the next experiments*. *For*

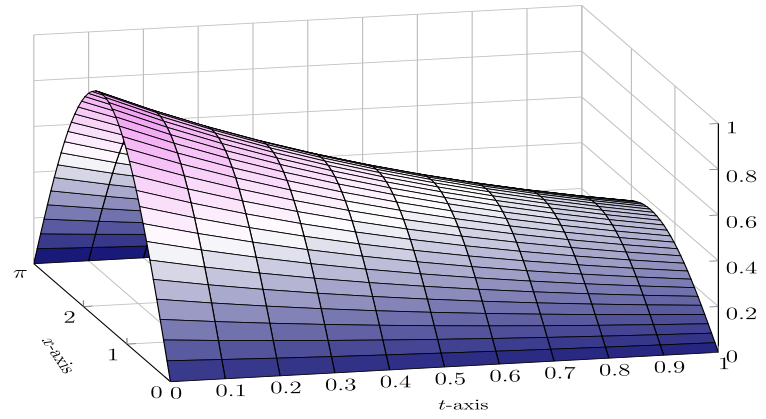

(a) $T_f = 1$

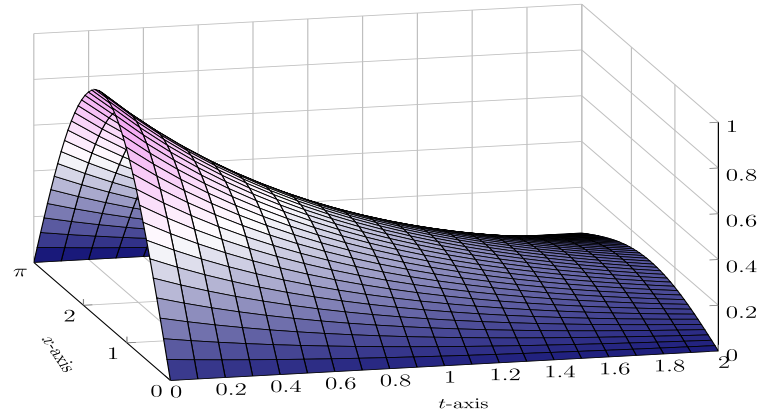

(b) $T_f = 2$

Figure 3 Plots of approximate solution for $T_f = 1$ (**a**) $T_f = 2$ (**b**) in Test Problem 5.2 for $\Delta t = 0.1, M = 8$

this purpose, we exploit the quartic B-spline collocation method (*QSCM*) [21], *the nonpolynomial spline method* (*NPSM*) [22], and *the improvised cubic B-spline collocation method* (*ICSCM*) [23].

The results using fixed $M = 15$ *and* $\Delta t = 0.01$, *and diverse values of* $T_f = 1, 2, 4, 10$ *are listed in Table 3. Clearly, our approach with less computational efforts is more accurate than the QSCM/ICSCM and is comparable with the NPSM.*

We next fix $M = 12$ *and vary* Δt *as* $1/2, 1/4, 1/8, 1/16$. *The estimated order of accuracy in time* (ROCt_∞) *is investigated at time* $T_f = 10$ *for this Test Problem as well. The results of achieved* $\mathcal{E}_\infty$ *error norms, together with related* ROCt_∞, *are shown in Table 4, where a further comparison with some other available computational methods is done.*

We have used the combined method based on a finite difference procedure and a new class of polynomials (FDCP) [28], the FDM [6], and the method based on Lucas polynomials [27]. Obviously, the presented results confirm that the order of accuracy of two is obtainable for the used time-marching algorithm and with relatively large time steps in comparison with other approaches.

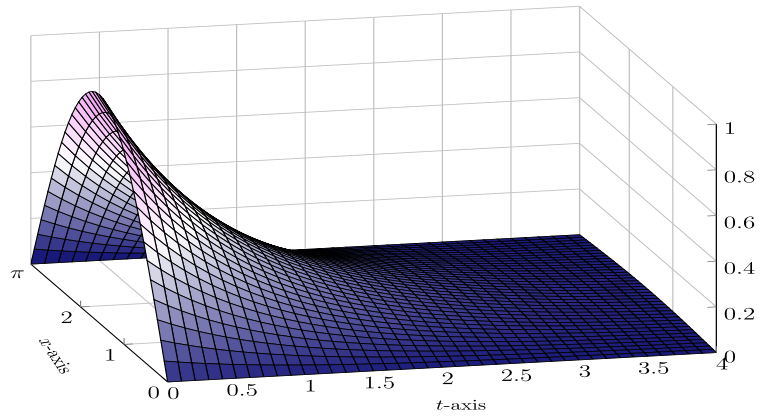

(a) $T_f = 1$

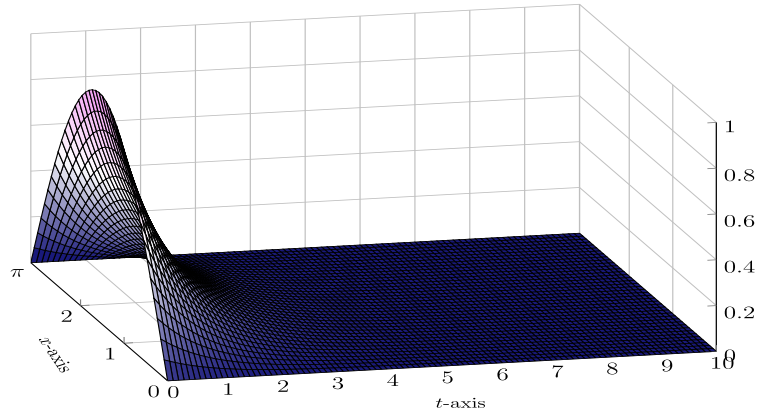

(b) $T_f = 2$

Figure 4 Plots of approximate solution for $T_f = 4$ (left) $T_f = 10$ (right) in Test Problem 5.2 for $\Delta t = 0.1, M = 8$

Test Problem 5.3 *The third test problem is devoted to the following nonhomogeneous model with nonunity coefficients* [27, 28], $\mu = 0.1, \gamma = 1, \sigma = 0.01, \eta = 1$:

$$h(x,t) = \left(\frac{9}{5} + \frac{189}{100}\left(x^2 - 1\right) + \frac{179}{50}x\right)e^{x-t} + \left(x^2 - 1\right)\left(x^2 + 2x - 1\right)e^{2x-2t}.$$

The computational domain is taken as

$$x \in [x_L, x_R] = [-1, 1], \quad t \in [0, T_f],$$

and the initial and boundary conditions are

$$\begin{cases} w(x,0) = e^x(1 - x^2), \\ w(x_L,t) = 0, \\ w(x_R,t) = 0. \end{cases}$$

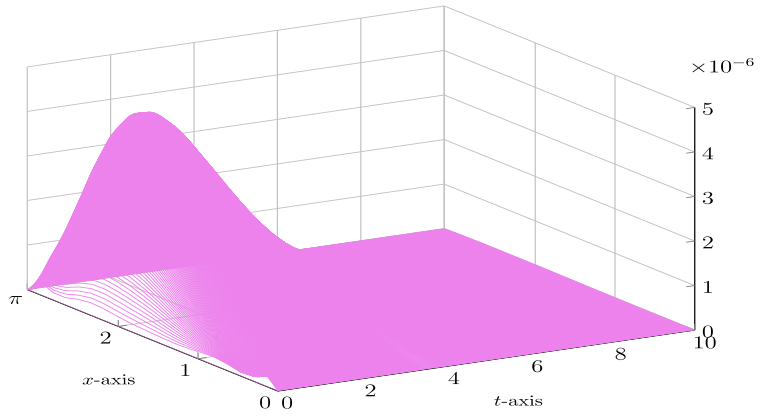

Figure 5 Plot of absolute errors in Test Problem 5.2 at different time instants $t = \ell\Delta t, \ell = 1, 2, \ldots, 10^3$, for $\Delta t = 0.01, M = 8$, and $T_f = 10$

Table 3 The comparison results of the L_∞ and L_2 error norms for Test Problem 5.2 using $M = 15$, $\Delta t = 0.01$, and various T_f

T_f	BTM ($M = 15$)		QSCM [21] ($N = 121$)	
	$\mathcal{E}_\infty$	$\mathcal{E}_2$	$\mathcal{E}_\infty$	$\mathcal{E}_2$
1	4.5054_{-6}	4.9885_{-6}	7.67_{-3}	5.13_{-3}
2	4.0853_{-6}	4.8560_{-6}	2.84_{-3}	1.73_{-3}
4	2.1470_{-6}	2.8457_{-6}	3.84_{-4}	2.12_{-4}
10	5.1292_{-7}	5.8866_{-7}	4.06_{-6}	4.08_{-6}
T_f	NPSM [22] ($N = 121$)		ICSCM [23] ($N = 40$)	
	$\mathcal{E}_\infty$	$\mathcal{E}_2$	$\mathcal{E}_\infty$	$\mathcal{E}_2$
1	4.4267_{-6}	4.7852_{-6}	1.4488_{-3}	1.5039_{-3}
2	3.6552_{-6}	4.0397_{-6}	1.1685_{-3}	1.2023_{-3}
4	1.3915_{-6}	1.5514_{-6}	3.9228_{-4}	3.9224_{-4}
10	2.4379_{-8}	2.4004_{-8}	3.1695_{-6}	2.7150_{-6}

The exact solution of this example is

$$w(x,t) = e^{x-t}\left(1 - x^2\right).$$

We first set $M = 8$ and $T_f = 1$ and use $\Delta t = 0.1$ in the computations. The approximate solution at $t = T_f$ on $[x_L, x_R]$ is obtained as

$$\begin{aligned}\mathcal{X}_{10,8}(x) = {} & -6.1430 \times 10^{-4}x^8 - 0.00321614x^7 - 0.0147067x^6 \\ & - 0.0578943x^5 - 0.168302x^4 - 0.306555x^3 \\ & - 0.18433x^2 + 0.367665x + 0.367954.\end{aligned}$$

The profiles of the approximate solutions along with related exact solutions at diverse time steps

$$t = \ell\Delta t, \quad \ell = 1, 2, \ldots, 10,$$

Table 4 The results of L_∞ error norms and the related temporal rates of convergence in Test Problem 5.2 with $M = 12$, $T_f = 10$, and diverse Δt

Δt	TBM ($M = 12$)	
	$\mathcal{E}_\infty$	ROCt_∞
$\frac{1}{2}$	1.7213_{-3}	–
$\frac{1}{4}$	4.2667_{-4}	2.0123
$\frac{1}{8}$	1.0575_{-4}	2.0124
$\frac{1}{16}$	2.5685_{-5}	2.0417

Δt	FDCP [28] ($N = 10$)			FDM [6]	Lucas [27]	
	τ	L_∞ (Reg)	L_∞ (CGL)	L_∞	L_∞ (Reg)	L_∞ (RegLin)
$\frac{1}{2}$	$\frac{1}{10}$	2.1255_{-5}	2.4317_{-6}	2.1800_{-2}	2.1292_{-5}	2.4317_{-6}
$\frac{1}{4}$	$\frac{1}{20}$	9.7989_{-6}	6.0862_{-7}	5.3000_{-3}	9.8171_{-6}	6.0857_{-7}
$\frac{1}{8}$	$\frac{1}{40}$	4.6914_{-6}	1.5231_{-7}	1.3000_{-3}	4.7005_{-6}	1.5215_{-7}
$\frac{1}{16}$	$\frac{1}{80}$	2.2936_{-6}	3.8081_{-8}	3.3291_{-4}	2.2981_{-6}	3.7998_{-8}

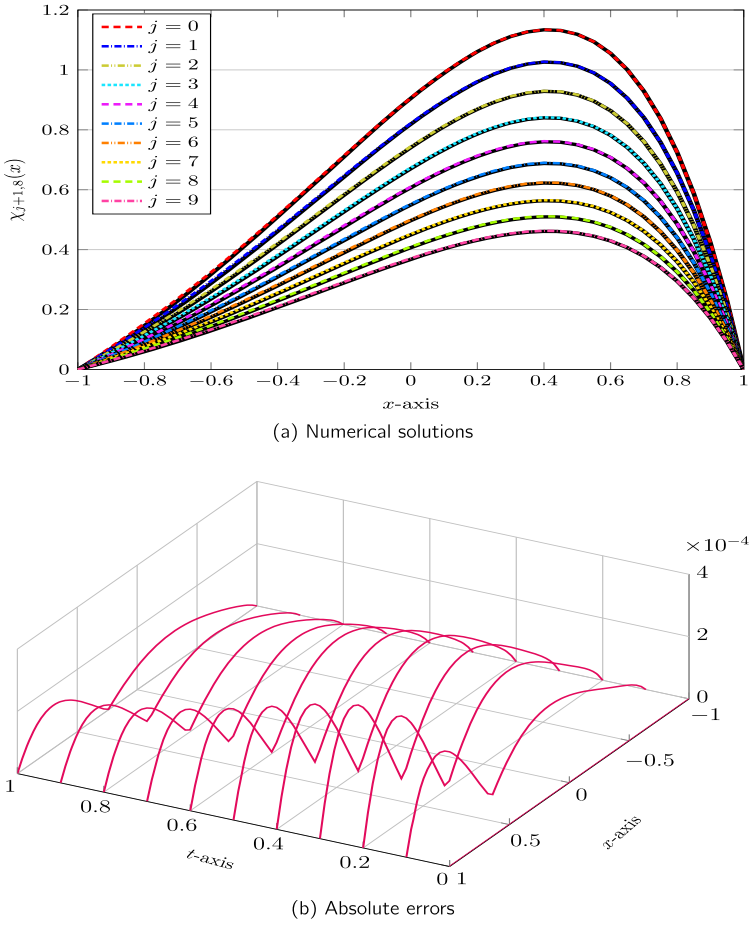

Figure 6 Plot of numerical solutions (**a**) and related absolute errors (**b**) in Test Problem 5.3 at $t = \ell \Delta t$, $\ell = 1, 2, \ldots, 10$, for $\Delta t = 0.1, M = 8$, and $T_f = 1$

are shown in Fig. 6, left. The related absolute errors are further shown in Fig. 6, right. In the next experiments, we indicate the second-order convergence of our approach with respect to time discretization. In Table 5, using $M = 10$ and various

Table 5 The results of L_∞ error norms and the related temporal rate of convergence in Test Problem 5.3 with $M = 10$, $T_f = 1$ and diverse Δt

Δt	TBM ($M = 10$)	
	$\mathcal{E}_\infty$	ROCt_∞
$\frac{1}{2}$	2.5261_{-3}	–
$\frac{1}{4}$	7.7570_{-4}	1.7033
$\frac{1}{8}$	1.9739_{-4}	1.9745
$\frac{1}{16}$	4.9553_{-5}	1.9940

Δt	FDCP [28]		CLM [26]		Lucas [27]
	τ	$L_\infty(N = 18)$	$L_\infty(N = 36)$	Order	$L_\infty(N = 18)$
$\frac{1}{2}$	$\frac{2}{10^3}$	5.0010_{-08}	2.048_{-07}	–	5.0011_{-08}
$\frac{1}{4}$	$\frac{1}{10^3}$	1.2502_{-08}	5.119_{-08}	2.00	1.2503_{-08}
$\frac{1}{8}$	$\frac{2}{10^4}$	5.0011_{-10}	2.047_{-09}	2.00	5.0014_{-10}
$\frac{1}{16}$	$\frac{1}{10^4}$	1.2496_{-10}	5.117_{-10}	2.00	1.2511_{-10}

$$\Delta t = 1/2^i, \quad i = 1, 2, 3, 4,$$

we present the achieved $\mathcal{E}_\infty$ and calculate the corresponding ROCt_∞. Similar results reported by other the existing schemes but with larger number of resources are also presented in Table 5. These approaches are the FDCP [28] with $N = 18$, the Chebyshev–Legendre method (CLM) [26] with $N = 36$, and the method based on Lucas polynomials [27] with $N = 18$. Clearly, the TBM using a few bases, together with relatively large time steps, confirms the order of convergence two.

The spectral accuracy with regard to the achieved $\mathcal{E}_2/\mathcal{E}_\infty$ error norms for the space variable is also investigated in Fig. 7. In these results, we have used $\Delta t = 10^{-3}$ and diverse

$$M = 2^i, \quad i = 1, 2, 3, 4.$$

The corresponding rates of convergence ROCx_2 and ROCx_∞ are also visualized in Fig. 7. Finally, for this test problem, let us see the behavior of numerical solution and error norms when $T_f = 5$. These results using $M = 12$ are depicted in Fig. 8. Note that in the left plot, we used $\Delta t = 0.05$ whereas for the right plotted absolute errors, we used $\Delta t = 0.005$. Additionally, the approximate solution for $\Delta t = 0.05$ on $x \in [-1, 1]$ at $t = T_f$ is given by

$$\begin{aligned}\mathcal{X}_{100,12}(x) = {} & -1.920 \times 10^{-9}x^{12} - 1.897 \times 10^{-8}x^{11} - 1.659 \times 10^{-7}x^{10} \\ & - 1.320 \times 10^{-6}x^9 - 9.196 \times 10^{-6}x^8 - 5.482 \times 10^{-5}x^7 \\ & - 2.714 \times 10^{-4}x^6 - 0.0010669x^5 - 0.0030883x^4 \\ & - 0.00561447x^3 - 0.00336744x^2 + 0.00673753x \\ & + 0.00673652.\end{aligned}$$

Test Problem 5.4 *In the last test problem, we pay attention to* [24, 25] *with* $\mu = 1, \gamma = 1, \sigma = 1$, *and* $\eta = \pm 1$. *For* $\eta = \pm 1$, *we have the right-hand side functions* $h(x, t)$, *respectively,*

$$\cosh^4(t - x)h(x, t) = -5\sinh(t - x) + 2\cosh(t - x) \pm \sinh(2t - 2x)/2$$

M	$\mathcal{E}_2$	$\mathcal{E}_\infty$
2^1	1.0783623×10^{-1}	2.4542623×10^{-1}
2^2	5.3756008×10^{-3}	1.9198625×10^{-2}
2^3	1.3250421×10^{-6}	6.8540817×10^{-6}
2^4	1.9556590×10^{-9}	1.2793891×10^{-8}

(a) $\mathcal{E}_2/\mathcal{E}_\infty$ errors

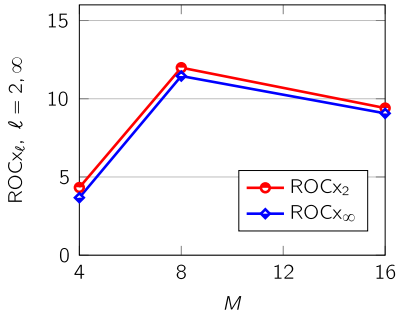

(b) Related rate of convergence

Figure 7 The results of $\mathcal{E}_2/\mathcal{E}_\infty$ errors (**a**) and related rate of convergence (**b**) in Test Problem 5.3 at $t = T_f$ for $\Delta t = 0.001$, $T_f = 1$, and various M

$$- \cosh^3(t-x) + \sinh^3(t-x).$$

The model problem (1) *is solved on*

$$x \in [x_L, x_R] = [0,1], [-1,1], \quad t \in [0, T_f].$$

The corresponding exact solution is

$$w(x,t) = \sec h(x-t).$$

The initial and boundary conditions are obtained from the exact solution for this example. We first consider $M = 7$ *and* $T_f = 1$ *and use* $\Delta t = 0.1$ *in the computations. The approximate solutions for* $\eta = \pm 1$ *at* $t = T_f$ *on* $[-1,1]$ *are obtained, respectively, as*

$$\begin{aligned}\mathcal{X}^+_{10,7}(x) = {} & 0.00842799x^7 + 0.0184003x^6 - 0.00867362x^5 \\ & - 0.0846306x^4 - 0.126626x^3 + 0.0502792x^2 \\ & + 0.49397x + 0.648852\end{aligned}$$

and

$$\begin{aligned}\mathcal{X}^-_{10,7}(x) = {} & 0.00869142x^7 + 0.018303x^6 - 0.00922897x^5 \\ & - 0.0843227x^4 - 0.126124x^3 + 0.0499579x^2 \\ & + 0.493761x + 0.648963.\end{aligned}$$

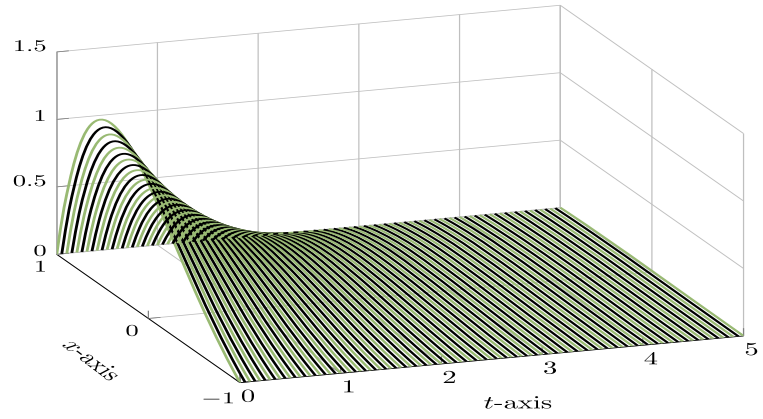

(a) Numerical solutions with $\Delta t = 0.05$

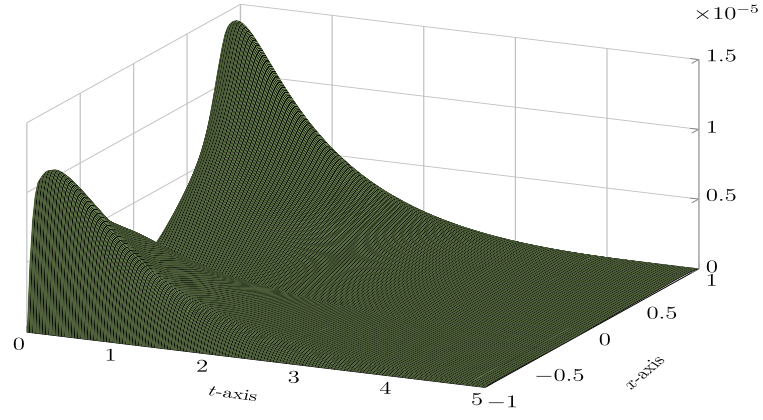

(b) Absolute errors with $\Delta t = 0.005$

Figure 8 Plot of numerical solutions with $\Delta t = 0.05$ (**a**) and graphs of absolute errors with $\Delta t = 0.005$ (**b**) in Test Problem 5.3 using $M = 12$ and $T_f = 5$

As we can see, both approximate solutions are very close to each other. We thus only plot the the graphs of $\mathcal{X}^{-}_{10,7}(x)$ *and the related absolute errors for* $\eta = -1$ *in Fig. 9.*

Next, we examine the behavior of $\mathcal{E}_\infty$ *error norms when* $M = 8$ *is fixed and* Δt *varies as* $1/2, 1/4, 1/8, 1/16$. *In addition, the final time is taken as* $T_f = 1$, *and* $[x_L, x_R] = [0, 1]$. *These results for* $\eta = -1$ *are reported in Table 6. For comparison, the outcomes of the previously existing computational procedures are also displayed in Table 5. To this end, we use the Lie-group approach based on radial basis functions* (*LG-RBFs*) [25], *the meshless method* [24], *and the Legendre spectral element method* (*LSEM*) [29]. *We can observe from the results shown in Table 6 that our numerical results provide second-order accuracy in time while employing a smaller number of bases and time steps compared to other well-established numerical procedures in the literature.*

Similar results for $\eta = +1$ *are further reported in Table 7. However, here we have used* $T_f = 0.1$, *and the values of* Δt *are* $1/10, 1/20, 1/40$ *as used in the results presented in the ICSCM* [23] *and meshless methods* [24] *with parameter* $h = 1/10$. *Clearly, the results obtained by the TBM are more accurate in comparison with two other methods. The next experiments show further the accuracy of our approach in the framework of results evaluated at time* $t = T_f$, *where* $T_f = 5$. *We use* $\eta = -1$ *and* $M = 8$ *and compare with the methods used in*

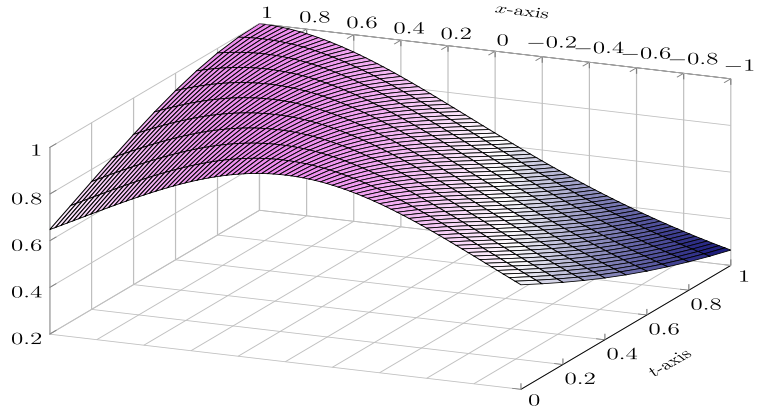

(a) Approximate solution

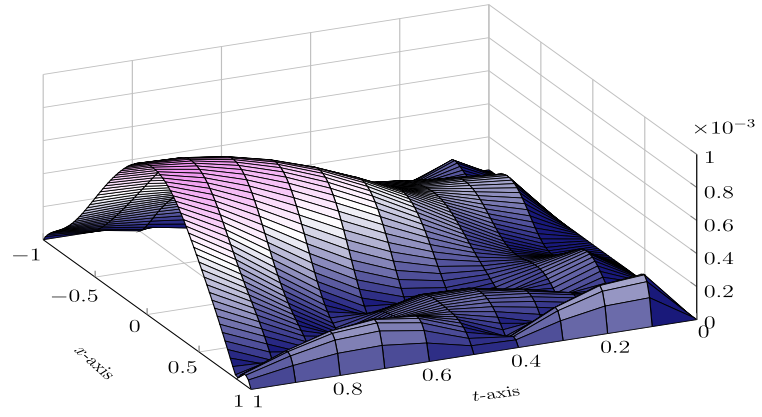

(b) Absolute errors

Figure 9 Plots of approximate solution (**a**) and absolute errors (**b**) in Test Problem 5.4 for $\Delta t = 0.1, M = 7$, $\eta = -1$, and $T_f = 1$

Table 6 The results of L_∞ error norms and the related temporal rate of convergence in Test Problem 5.4 with $M = 8$, $T_f = 1$, $\eta = -1$, and diverse Δt on $[0, 1]$

Δt	TBM ($M = 8$)	
	$\mathcal{E}_\infty$	ROCt_∞
$\frac{1}{2}$	4.9238_{-3}	–
$\frac{1}{4}$	1.2592_{-3}	1.9672
$\frac{1}{8}$	3.1642_{-4}	1.9926
$\frac{1}{16}$	7.9514_{-5}	1.9925

Δt	LG-RBFs [25]		LSEM [29]		Meshless [24]
	τ	$dx = 0.1$	$N_e = 20, p_e = 5$	C-order	$dx = 0.1$
$\frac{1}{2}$	$\frac{1}{10}$	1.1899_{-2}	5.8541_{-4}	–	1.1306_{-2}
$\frac{1}{4}$	$\frac{1}{20}$	6.4885_{-3}	2.4834_{-4}	0.9974	5.6005_{-3}
$\frac{1}{8}$	$\frac{1}{40}$	3.2224_{-3}	1.1379_{-4}	0.9986	2.7770_{-3}
$\frac{1}{16}$	$\frac{1}{80}$	1.6079_{-3}	5.4413_{-5}	0.9992	1.3862_{-3}

Table 6. The aforementioned results are shown in Table 8, which indicate the superiority of our procedure compared to the LG-RBFs, LSEM, and meshless approaches. Besides, the second-order accuracy in time is visible from the given results if Table 8. For completeness,

Table 7 The results of L_∞ error norms and the related temporal rate of convergence in Test Problem 5.4 with $M = 8$, $T_f = 0.1$, $\eta = +1$, and diverse Δt on $[0, 1]$

Δt	TBM ($M = 8$)			
	$\mathcal{E}_2$	ROCt_2	$\mathcal{E}_\infty$	ROCt_∞
$\frac{1}{10}$	1.5275_{-6}	–	8.8717_{-5}	–
$\frac{1}{20}$	2.5300_{-7}	2.5939	2.1601_{-5}	2.0381
$\frac{1}{40}$	8.8279_{-8}	1.5190	4.9149_{-6}	2.1359

Δt	ICSCM [23]		Meshless [24]	
	L_2	L_∞	L_2	L_∞
$\frac{1}{10}$	3.1380_{-4}	5.2316_{-4}	4.8125_{-3}	2.4109_{-3}
$\frac{1}{20}$	1.6563_{-4}	2.7764_{-4}	2.3406_{-3}	1.1911_{-3}
$\frac{1}{40}$	8.5147_{-5}	1.4284_{-4}	1.1793_{-3}	6.0771_{-4}

Table 8 The results of L_∞ error norms and the related temporal rate of convergence in Test Problem 5.4 with $M = 8$, $T_f = 5$, $\eta = -1$, and diverse Δt on $[0, 1]$

Δt	TBM ($M = 8$)		LG-RBFs [25]
	$\mathcal{E}_\infty$	ROCt_∞	$dx = 0.1$
$\frac{1}{10}$	8.3562_{-6}	–	5.4835_{-4}
$\frac{1}{20}$	2.0867_{-6}	2.0016	2.8818_{-4}
$\frac{1}{40}$	5.2139_{-7}	2.0008	1.5032_{-4}
$\frac{1}{80}$	1.3018_{-7}	2.0019	7.7388_{-5}

Δt	LSEM [29]		Meshless [24]
	$N_e = 20, p_e = 5$	C-order	$dx = 0.1$
$\frac{1}{10}$	2.4232_{-4}	–	1.0335_{-3}
$\frac{1}{20}$	1.2138_{-4}	0.9974	5.8509_{-4}
$\frac{1}{40}$	6.0748_{-5}	0.9986	2.9635_{-4}
$\frac{1}{80}$	3.0390_{-5}	0.9992	1.4801_{-4}

the graphical representations of approximate solutions together with their absolute errors at diverse time instants

$$t = \ell \Delta t, \quad s = 1, 2, \ldots, 50,$$

are visualized in Fig. 10. Finally, for the last test example, we also investigate the spectral accuracy of the numerical solutions for $\Delta t = 0.001$ *and moderate values of*

$$M = 2^i, \quad i = 1, 2, 3, 4.$$

For the simulations, we employ both $\eta = \pm 1$ *and compute the results at* $T_f = 1$ *and the spatial domain* $[-1, 1]$. *The results are shown in Table 9.*

6 Conclusions

We have developed an accurate time numerical solution algorithm (using a large time step) for the generalized BBMB-type equations (1) arising in diverse disciplines of engineering science. The proposed technique is constructed based on a combination of the Boubaker collocation procedure for the spatial variable and the Taylor series formula for the temporal discretization. The main characteristic of the presented work is that we need to solve an algebraic system of equations at each time step rather than solving a global system obtained in the spectral collocation methods developed in the past. The convergence analysis of the hybrid technique is discussed. The numerical results shown in tables and

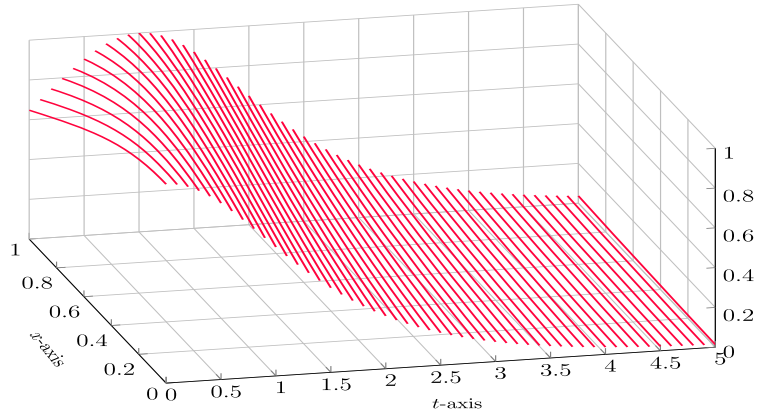

(a) Approximate solutions

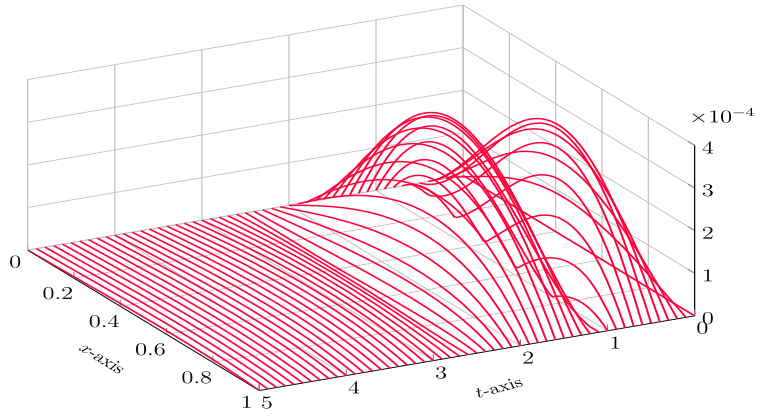

(b) Absolute errors

Figure 10 Plot of approximate solutions (**a**) and absolute errors (**b**) in Test Problem 5.4 for $\Delta t = 0.1, M = 8$, $\eta = -1$, and $T_f = 5$

Table 9 The results of $\mathcal{E}_2/\mathcal{E}_\infty$ error norms and the related spatial rate of convergence in Test Problem 5.4 with $\Delta t = 0.001$, $T_f = 1$, $\eta = \pm 1$, and diverse M on $[-1, 1]$

M	$\eta = -1$			
	$\mathcal{E}_2$	ROCx_2	$\mathcal{E}_\infty$	ROCx_∞
2	3.8426_{-2}	–	8.6267_{-2}	–
4	2.8716_{-3}	3.7421	8.3279_{-3}	3.3728
8	6.4843_{-5}	5.4688	3.1262_{-4}	4.7355
16	2.8165_{-8}	11.169	1.3819_{-7}	11.144
M	$\eta = +1$			
	$\mathcal{E}_2$	ROCx_2	$\mathcal{E}_\infty$	ROCx_∞
2	1.9233_{-2}	–	5.0755_{-2}	–
4	9.1990_{-4}	4.3860	3.8484_{-3}	3.7212
8	7.8660_{-5}	3.5478	3.4115_{-4}	3.4958
16	1.9247_{-8}	11.997	8.8667_{-8}	11.910

figures justify the second-order accuracy in time and the high-order accuracy in the space of the presented technique in comparison with some existing well-established computational schemes.

Acknowledgements
Not applicable.

Funding
Not applicable.

Availability of data and materials
Data sharing not applicable to this paper as no datasets were generated or analyzed during the current study.

Declarations

Ethics approval and consent to participate
Not applicable.

Consent for publication
Not applicable.

Competing interests
The authors declare that they have no competing interests.

Authors' contributions
The authors declare that the study was realized in collaboration with equal responsibility. Both authors read and approved the final manuscript.

Author details
[1]Department of Applied Mathematics, Faculty of Mathematics and Computer, Shahid Bahonar University of Kerman, Kerman, Iran. [2]Department of Mathematics, Bu-Ali Sina University, Hamedan, Iran.

Publisher's Note

Received: 3 February 2022 Accepted: 14 March 2022 Published online: 01 April 2022

References

1. Mei, M.: Large-time behavior of solution for generalized Benjamin–Bbona–Mahony–Burgers equations. Nonlinear Anal. **33**, 699–714 (1998)
2. Benjamin, T.B., Bona, J.L., Mahony, J.J.: Model equations for long waves in nonlinear dispersive systems. Philos. Trans. R. Soc. Lond. A **272**, 47–78 (1972)
3. Peregrine, D.H.: Calculations of the development of an undular bore. J. Fluid Mech. **25**, 321–330 (1966)
4. Izadi, M., Yüzbasbi, S., Baleanu, D.: A Taylor–Chebyshev approximation technique to solve the 1D and 2D nonlinear Burgers equations. Math. Sci. (2021). https://doi.org/10.1007/s40096-021-00433-1
5. Bona, J.L.: Model equations for waves in nonlinear dispersive systems. In: Proc. Int. Congress of Mathematicians, Helsinki, vol. 2, pp. 887–894 (1978)
6. Omrani, K., Ayadi, M.: Finite difference discretization of the Benjamin–Bbona–Mahony–Burgers equation. Numer. Methods Partial Differ. Equ. **24**, 239–248 (2008)
7. Bayarassou, K.: Fourth-order accurate difference schemes for solving Benjamin–Bona–Mahony–Burgers (BBMB) equation. Eng. Comput. **37**, 123–138 (2021). https://doi.org/10.1007/s00366-019-00812-2
8. Etemad, S.T.M.T., Etemad, S., Rezapour, S.: On a coupled Caputo conformable system of pantograph problems. Turk. J. Math. **45**(1), 496–519 (2020)
9. Mohammadi, H., Kumar, S., Rezapour, S., Etemad, S.: A theoretical study of the Caputo–Fabrizio fractional modeling for hearing loss due to Mumps virus with optimal control. Chaos Solitons Fractals **144**, Article ID 110668 (2021)
10. Alizadeh, S., Baleanu, D., Rezapour, S.: Analyzing transient response of the parallel RCL circuit by using the Caputo–Fabrizio fractional derivative. Adv. Differ. Equ. **2020**, Article ID 55 (2020)
11. Samei, M.E., Rezapour, S.: On a system of fractional q-differential inclusions via sum of two multi-term functions on a time scale. Bound. Value Probl. **2020**, Article ID 135 (2020)
12. Samei, M.E., Hedayati, V., Rezapour, S.: Existence results for a fraction hybrid differential inclusion with Caputo–Hadamard type fractional derivative. Adv. Differ. Equ. **2019**, Article ID 163 (2019). https://doi.org/10.1186/s13662-019-2090-8
13. Abdeljawad, T., Samei, M.E.: Applying quantum calculus for the existence of solution of q-integro-differential equations with three criteria. Discrete Contin. Dyn. Syst., Ser. S **14**(10), 3351–3386 (2021)
14. Balanu, D., Mohammadi, H., Rezapour, S.: Analysis of the model of HIV-1 infection of $cd4^+$ t-cell with a new approach of fractional derivative. Adv. Differ. Equ. **2020**, Article ID 71 (2020)
15. Baleanu, D., Etemad, S., Pourrazi, S., Rezapour, S.: On the new fractional hybrid boundary value problems with three-point integral hybrid conditions. Adv. Differ. Equ. **2019**, Article ID 473 (2019)
16. Baleanu, D., Hedayati, V., Rezapour, S., Mohamed Al Qurashi, M.: On two fractional differential inclusions. SpringerPlus **5**(1), 882 (2016)
17. Baleanu, D., Etemad, S., Rezapour, S.: On a fractional hybrid integro-differential equation with mixed hybrid integral boundary value conditions by using three operators. Alex. Eng. J. **59**(5), 3019–3027 (2020)
18. Raupp, M.A.: Galerkin methods applied to the Benjamin–Bona–Mahony equation. Bol. Soc. Brazil Math. **6**, 65–77 (1975)

19. Wahlbin, L.: Error estimates for a Galerkin method for a class of model equations for long waves. Numer. Math. **23**, 289–303 (1975)
20. Izadi, M.: Application of the Newton–Raphson method in a SDFEM for inviscid Burgers equation. Comput. Methods Differ. Equ. **8**(4), 708–732 (2020)
21. Arora, G., Mittal, R.C., Singh, B.K.: Numerical solution of BBM–Burger equation with quadratic b-spline collocation method. J. Eng. Sci. Technol. **9**, 104–116 (2014)
22. Kanth, A.R., Deepika, S.: Non-polynomial spline method for one dimensional nonlinear Benjamin–Bona–Mahony–Burgers equation. Int. J. Nonlinear Sci. Numer. Simul. **18**(3–4), 277–284 (2017)
23. Shallu, V.K.K.: Numerical treatment of Benjamin–Bona–Mahony–Burgers equation with fourth-order improvised b-spline collocation method. J. Ocean Eng. Sci. (2021). https://doi.org/10.1016/j.joes.2021.07.001
24. Dehghan, M., Abbaszadeh, M., Mohebbi, A.: The numerical solution of nonlinear high dimensional generalized Benjamin–Bona–Mahony–Burgers equation via the meshless method of radial basis functions. Comput. Math. Appl. **68**, 212–237 (2014)
25. Hajiketabi, M., Abbasbandy, S., Casas, F.: The Lie-group method based on radial basis functions for solving nonlinear high dimensional generalized Benjamin–Bona–Mahony–Burgers equation in arbitrary domains. Appl. Math. Comput. **321**, 223–243 (2018)
26. Zhao, T., Zhang, X., Huo, J., Su, W., Liu, Y., Wu, Y.: Optimal error estimate of Chebyshev–Legendre spectral method for the generalised Benjamin–Bona–Mahony–Burgers equations. Abstr. Appl. Anal. **2012**, Article ID 106343 (2012)
27. Oruc, O.: A new algorithm based on Lucas polynomials for approximate solution of 1D and 2D nonlinear generalized Benjamin–Bona–Mahony–Burgers equation. Comput. Math. Appl. **74**, 3042–3057 (2017)
28. Hajishafieiha, J., Abbasbandy, S.: A new class of polynomial functions for approximate solution of generalized Benjamin–Bona–Mahony–Burgers (gBBMB) equations. Appl. Math. Comput. **367**, Article ID 124765 (2020)
29. Dehghan, M., Shafieeabyaneh, N., Abbaszadeh, M.: Numerical and theoretical discussions for solving nonlinear generalized Benjamin–Bona–Mahony–Burgers equation based on the Legendre spectral element method. Numer. Methods Partial Differ. Equ. **37**(1), 360–382 (2021)
30. Yüzbasi, Ş.: A collocation approach for solving two-dimensional second-order linear hyperbolic equations. Appl. Math. Comput. **338**, 101–114 (2018)
31. Karpinar, Z., Baleanu, D., Inc, M., Almohsen, B.: Some applications of the least squares-residual power series method for fractional generalized long wave equations. J. Ocean Eng. Sci. (2022). https://doi.org/10.1016/j.joes.2021.09.001
32. Izadi, M., Srivastava, H.M.: An optimized second order numerical scheme applied to the non-linear Fisher's reaction–diffusion equation. J. Interdiscip. Math. **25**, 471–492 (2022). https://doi.org/10.1080/09720502.2021.1930662
33. Mishra, S.K., Rajković, P., Samei, M.E., Chakraborty, S.K., Ram, B., Kaabar, M.K.A.: A q-gradient descent algorithm with quasi-Fejér convergence for unconstrained optimization problems. Fractal Fract. **5**(2), 110 (2021). https://doi.org/10.3390/fractalfract5030110
34. Mishra, S.K., Samei, M.E., Chakraborty, S.K., Ram, B.: On q-variant of Dai–Yyuan conjugate gradient algorithm for unconstrained optimization problems. Nonlinear Dyn. **104**, 2471–2496 (2021). https://doi.org/10.1007/s11071-021-06378-3
35. Mishra, S.K., Chakraborty, S.K., Samei, M.E., Ram, B.: q-Polak–Ribière–Polyak conjugate gradient algorithm for unconstrained optimization problems. J. Inequal. Appl. **2021**, Article ID 25 (2021). https://doi.org/10.1186/s13660-021-02554-6
36. Hosseininia, M., Heydari, M.H., Cattani, C.: A wavelet method for nonlinear variable-order time fractional 2D Schrödinger equation. Discrete Contin. Dyn. Syst., Ser. S **14**(7), 2273–2295 (2021)
37. Mishra, S.K., Panda, G., Chakraborty, S.K., Samei, M.E., Ram, B.: On q-BFGS algorithm for unconstrained optimization problems. Adv. Differ. Equ. **2020**, Article ID 638 (2020). https://doi.org/10.1186/s13662-020-03100-2
38. Lai, K.K., Mishra, S.K., Panda, G., Chakraborty, S.K., Samei, M.E., Ram, B.: A limited memory q-BFGS algorithm for unconstrained optimization problems. J. Appl. Math. Comput. **6663**, 183–202 (2021). https://doi.org/10.1007/s12190-020-01432-6
39. Izadi, M.: A second-order accurate finite-difference scheme for the classical Fisher–Kolmogorov–Petrovsky–Piscounov equation. J. Inf. Optim. Sci. **42**(2), 431–448 (2021). https://doi.org/10.1186/s13662-020-03100-2
40. Rezazadeh, H., Inc, M., Baleanu, D.: New solitary wave solutions for variants of (3 + 1)-dimensional Wazwaz–Benjamin–Bona–Mahony equations. Front. Phys. (2020). https://doi.org/10.3389/fphy.2020.00332
41. Javeed, S., Saif, S., Waheed, A., Baleanu, D.: Exact solutions of fractional mbbm equation and coupled system of fractional Boussinesq–Burgers. Results Phys. **9**, 1275–1281 (2018)
42. Izadi, M.: Numerical approximation of Hunter–Saxton equation by an efficient accurate approach on long time domains. UPB Sci. Bull., Ser. A **83**(1), 291–300 (2021)
43. Izadi, M.: A combined approximation method for nonlinear foam drainage equation. Sci. Iran. **29**(1), 70–78 (2022). https://doi.org/10.24200/sci.2021.56571.4792
44. Izadi, M., Yüzbas, S.: A hybrid approximation scheme for 1-d singularly perturbed parabolic convection–diffusion problems. Math. Commun. **27**(1), 47–63 (2022). https://doi.org/10.24200/sci.2021.56571.4792
45. Kaabar, M.K.A., Kaplan, M., Siri, Z.: New exact soliton solutions of the (3 + 1)-dimensional conformable Wazwaz–Benjamin–Bona–Mahony equation via two novel techniques. J. Funct. Spaces (2021). https://doi.org/10.1155/2021/4659905
46. Matar, M.M., Abbas, M.I., Alzabut, J., Kaabar, M.K.A., Etemad, S., Rezapour, S.: Investigation of the p-Laplacian nonperiodic nonlinear boundary value problem via generalized Caputo fractional derivatives. Adv. Differ. Equ. **2021**, Article ID 68 (2021). https://doi.org/10.1186/s13662-021-03228-9
47. Kaabar, M.K.A., Refice, A., Souid, M.S., Martínez, F., Etemad, S., Siri, Z., Rezapour, S.: Existence and UHR stability of solutions to the implicit nonlinear FBVP in the variable order settings. Mathematics **9**, 1693 (2021). https://doi.org/10.3390/math9141693
48. Matar, M.M., Abbas, M.I., Alzabut, J., Kaabar, M.K.A., Etemad, S., Rezapour, S.: Investigation of the p-Laplacian nonperiodic nonlinear boundary value problem via generalized Caputo fractional derivatives. Adv. Differ. Equ. **2021**, Article ID 68 (2021)

49. Kaabar, M.K.A., Shabibi, M., Alzabut, J., Etemad, S., Sudsutad, W., Martínez, F., Rezapour, S.: Investigation of the fractional strongly singular thermostat model via fixed point techniques. Mathematics **9**, 2298 (2021). https://doi.org/10.3390/math9182298
50. Achar, S.J., Baishya, C., Kaabar, M.K.A.: Dynamics of the worm transmission in wireless sensor network in the framework of fractional derivatives. Math. Methods Appl. Sci. (2021). https://doi.org/10.1002/mma.8039
51. Abu-Shady, M., Kaabar, M.K.A.: A generalized definition of the fractional derivative with applications. Math. Probl. Eng. **9**, 2298 (2021). https://doi.org/10.3390/math9182298
52. Rezapour, S., Samei, M.E.: On the existence of solutions for a multi-singular point-wise defined fractional q-integro-differential equation. Bound. Value Probl. **2020**, Article ID 38 (2020). https://doi.org/10.1186/s13661-020-01342-3
53. Abdelwahed, M., Chorfi, N.: A posteriori analysis of the spectral element discretization of a non linear heat equation. Adv. Nonlinear Anal. **10**(1), 477–493 (2021). https://doi.org/10.3390/math9182298
54. Chorfi, N., Abdelwahed, M., Berselli, L.: On the analysis of a geometrically selective turbulence model. Adv. Nonlinear Anal. **9**(1), 1402–1419 (2020). https://doi.org/10.3390/math9182298
55. Boubaker, K.: On modified boubaker polynomials: some differential and analytical properties of the new polynomial issued from an attempt for solving bi-varied heat equation. Trends Appl. Sci. Res. **2**, 540–544 (2007)
56. Kim, S.H., Zhang, L., Boubaker, K., Lei, Q.: On zeros of Boubaker polynomials. Bull. Korean Math. Soc. **51**(2), 547–553 (2014)
57. Parand, K., Yousefi, H., Fotouhifar, M., Delkhosh, M., Hosseinzadeh, M.: Shifted Boubaker Lagrangian approach for solving biological systems. Int. J. Biomath. **11**(3), Article ID 1850039 (2018)
58. Stewart, G.W.: Afternotes on Numerical Analysis, vol. 49 SIAM, Philadelphia (1996)